Combustion and Flame 269 (2024) 113683

Contents lists available at ScienceDirect

Combustion and Flame

journal homepage: www.sciencedirect.com/journal/combustion-and-flame

Modeling smothering limit of smoldering combustion: Oxygen supply, fuel density, and moisture content

Yunzhu Qin [a], Yuying Chen [a], Yichao Zhang [a], Shaorun Lin [b,*], Xinyan Huang [a,*]

[a] Research Centre for Smart Urban Resilience and Firefighting, The Hong Kong Polytechnic University, Kowloon, Hong Kong SAR
[b] Department of Mechanical Engineering, University of California, Berkeley, CA, United States

ARTICLE INFO

Keywords:
Smoldering limits
Internal airflow
Numerical simulation
Fuel properties
Extinction limits

ABSTRACT

Smoldering, characterized as a slow, low-temperature, and flameless reaction process, represents one of the most persistent types of combustion phenomena. While oxygen supply is one of the governing mechanisms controlling smoldering, the specific oxygen threshold or smothering limit remains inadequately investigated. Herein, we built a physics-based 1-D computational model integrating heat-and-mass transfer and 5-step heterogeneous chemistry to investigate the oxygen threshold or smothering limit of smoldering propagation in porous pine needle beds subjected to forced internal oxidizer flow. Simulation results revealed that, the required oxidizer flow velocity or oxygen supply rate increased as the oxygen concentration decreased, and the predicted limiting oxygen concentration (LOC) was about 3 %, agreeing well with the experimental observations and theoretical analysis. Moreover, the required airflow velocity was predicted to increase as the fuel density and environmental temperature decreased, or the moisture content increased, and the predicted maximum moisture content capable of supporting smoldering was about 110 %. At the smothering limit, the modeled minimum smoldering temperature and propagation rate were around 300 °C and 0.5 cm/h. This work helps deepen our understanding of the limiting conditions of smoldering combustion, thus improving the mitigation strategy of smoldering fire and the efficiency of applied smoldering systems.

Novelty and significance statements: Oxygen supply is one of the key mechanisms governing the smoldering propagation. In the literature, scattered studies have examined the limiting oxygen concentration (LOC) of smoldering under different conditions, leading to disparate results even for the same fuels. In our previous work, for the first time, we developed a tubular smoldering reactor capable of precisely controlling the flow of oxidizer, and successfully quantified the exact oxygen supply limit of smoldering combustion. However, no computational model was established specifically for the oxygen threshold of smoldering with forced internal oxygen supply. The novelty of this research is the establishment of the first-ever computational model to investigate the oxygen threshold or smothering limit of smoldering propagation in porous pine needle beds subjected to forced internal oxidizer flow. It is significant because (1) it contributes to a fundamental understanding of smoldering combustion; (2) it investigates the role of fuel properties and environmental conditions in smoldering dynamics and the oxygen supply limits; (3) it assists in optimizing the applied smoldering systems and enriching prevention strategies for smoldering fires.

1. Introduction

Smoldering, characterized by its slow, low-temperature, and flameless nature, is one of the most persistent types of combustion phenomena [1–4]. This intricate process is sustained when oxygen molecules directly attack the hot surface of reactive porous media, involving a multitude of elementary chemical reactions coupled with complex heat-and-mass transfer mechanisms [5,6]. Smoldering combustion exhibits a dual nature, presenting both destructive and constructive potentials. On the one hand, it poses catastrophic risks to natural environments such as peatlands, coal seams, and forest litter layers [3,7–9], and serves as a primary contributor to residential fires [10,11]. On the other hand, well-controlled applied smoldering processes offer promising avenues for syngas production [12], waste remediation [13], and pollution control [14], playing an important role in the context of our increasing attention to resources, energy, and environment. Therefore, gaining a deeper understanding of the fundamental principles of

* Corresponding authors.
E-mail addresses: shaorun.lin@berkeley.edu (S. Lin), xy.huang@polyu.edu.hk (X. Huang).

https://doi.org/10.1016/j.combustflame.2024.113683
Received 7 May 2024; Received in revised form 16 August 2024; Accepted 16 August 2024
Available online 22 August 2024

Nomenclature

Symbols

A	condensed phase species A (reactant)
B	condensed phase species B (product)
c	specific heat capacity (J/kg K)
D	diffusivity (m^2/s) /pore size (m)
d_p	characteristic pore size (m)
E	activation energy (J)
F	fuel (−)
ΔH	heat of reaction (MJ/kg)
h	specific enthalpy (J/kg)
h_c	convective coefficient (W/m^2 K)
h_r	radiative coefficient (W/m^2 K)
K	permeability (m^2)
k	thermal conductivity (W/m K)
L	fuel length
M	molar mass (g/mol)
m	mass (g)
$\dot{m}''$	mass flux (g/m^2 s)
Nu	Nusselt number (−)
n_k	reaction order (−)
p	pressure (Pa)
$\dot{q}''$	heat flux (kW/m^2)
S	spread/surface area (m^2)
T	temperature (°C)
t	time (s)
U	flow velocity (mm/s)
X	volume fraction (−)
Y	mass fraction (−)
Z	pre-exponential factor (s^{-1})
ΔZ	cell size (m)

Abbreviations

MC	moisture content
LOC	limiting oxygen concentration

Greeks

α	thermal diffusivity (m^2/s)
γ	radiative conductivity coefficient (m)
ε	emissivity (−)
ν	viscosity/stochiometric factor (Pa s/−)
ρ	density (kg/m^3)
σ	Stefan–Boltzmann constant (kg/s3 K4)
ψ	porosity (−)
$\dot{\omega}''$	volumetric reaction rate (kg/m^3 s)

Subscripts

cond	conduction
conv	convection
cp	cellulose pyrolysis
d	destruction
dr	drying process
e	environmental
ev	evaporation
f	formation
g	gas
hp	hemicellulose pyrolysis
i	species number
k	reaction number
min	minimum
lp	lignin pyrolysis
o	original/bulk
O_2	oxygen
ox	oxidation or oxidizer
r	radiation
s	solid
sm	smoldering
lp	lignin pyrolysis
∞	ambient

smoldering combustion is crucial.

Smoldering combustion is governed by the competition between oxygen supply and heat loss [2]. Previous studies have explored the effects of heat loss on the smoldering propagation through both experimental [13,15] and numerical approaches [16], providing a necessary foundation for hazard mitigation and optimization of industrial applications. Oxygen also plays a crucial role in heterogeneous oxidations, releasing heat to balance endothermic processes including pre-heating, drying and pyrolysis reactions, as well as environmental cooling [17]. Consequently, the oxygen threshold and smothering limit of smoldering combustion are highly important for determining the criteria of smoldering ignition, propagation, and extinction [18,19]. However, our understanding of the oxygen threshold (smothering limit) of self-sustaining smoldering and the underlying mechanisms remains relatively limited.

In the literature, scattered studies have examined the limiting oxygen concentration (LOC) of smoldering combustion of different biomass fuels under various conditions, including external wind or quiescent ambient environments. These studies have yielded disparate results, with reported LOC values ranging from 10 % [20], 13 % [21], and 16 % [22] for peat, 4 % [19] for wood, to 13.5 % [23] for cellulosic material. However, as the diffusion of oxygen from the surroundings cannot be completely isolated in the aforementioned studies, the precise amount of oxygen that penetrated the porous fuel remained undetermined. To fill this gap, our recent study [24] developed a tubular smoldering reactor capable of precisely controlling the flow of oxidizer with a prescribed oxygen concentration and flow rate through the porous media. We found that, for high organic porous fuel (e.g., peat), the LOC could be <2 %, and the minimum internal oxygen supply rate was approximately 0.08 ± 0.01 g/m^2·s. However, the oxygen threshold of pine needles, a more representative forest litter prone to smoldering combustion, has not yet been reported. Meanwhile, LOC for smoldering of porous fuels is complex that would be influenced by many factors such as the inherent physicochemical properties of the fuels (e.g., density, moisture content, and inorganic content) and environmental conditions (e.g., system heat loss, environment temperature, and even gravity), requiring further investigations [25–27].

Pine needle litter is a common wildland fuel in coniferous forests prone to fires [28,29]. It often forms highly porous fuel beds that can ignite a smoldering fire with a lower energy input and subsequently transition to flaming fires (StF) under natural wind, posing significant hazards [30,31]. Despite many studies have experimentally and numerically investigated the pine needles and other litters (e.g., duff and mulch) in terms of smoldering kinetics [32], smoldering ignition [33], smoldering propagation [34–36], flammability [31], and StF transition [30,37], the role of oxygen supply in their near-limit smoldering combustion is still poorly understood. For the first time, our previous work experimentally investigated the minimum oxygen supply rate of smoldering propagation over pine needle beds and quantified the effects of bulk density [38], but the effect of other physicochemical properties of the fuels and environmental conditions are still unknown. Furthermore, to the best of the authors' knowledge, no computational model has been established specifically for the oxygen threshold and smothering limit of smoldering combustion with forced internal oxygen supply, highlighting

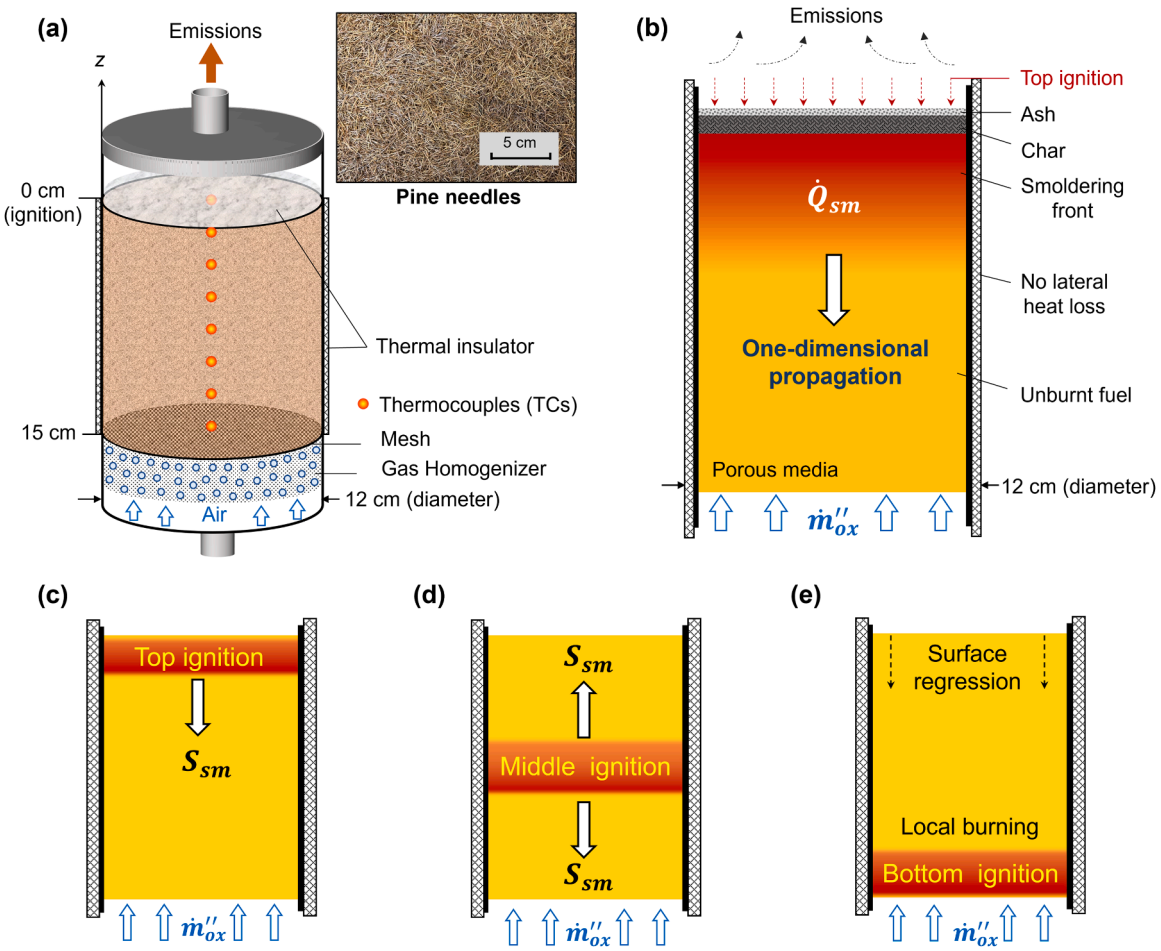

Fig. 1. (a) Experimental setup to explore the oxygen supply thresholds (or smothering limits) of smoldering combustion, where pine needles were selected as representative porous fuel; (b) schematic diagram of the one-dimensional smoldering model; (c–e) common ignition locations (top, middle, and bottom ignition protocol) used in the studies of in vertical smoldering propagation.

a huge knowledge gap.

To address these knowledge gaps, this work built a 1-D computational model for smoldering combustion based on open-source code Gpyro [39] and a previously developed 5-step smoldering kinetics of smoldering pine needles [40]. Oxygen was supplied as a forced internal oxidizer flow within porous fuels. Numerical simulations were performed to investigate the oxygen threshold or smothering limits specifically for smoldering combustion of pine needle beds as well as smoldering dynamics under different oxygen supply, and then verify the previous experiments and theoretical analysis. Moreover, the effects of fuel properties (moisture contents and bulk densities) and environmental conditions (oxygen concentrations and ambient temperatures) on the smoldering dynamics were also explored.

2. Computational model

2.1. Experiment description and model establishment

Most existing studies related to the smothering limits of smoldering were conducted under conditions of external wind or in a quiescent surrounding environment [19–22], making it difficult to quantify the specific amount of oxygen required for smoldering combustion. To address this, our latest experiment designed an enclosed tubular smoldering reactor to regulate the prescribed airflow feeding the smoldering combustion [24,38]. Because the experiments used to verify our model were conducted using this tubular reactor, a brief description of the experimental setup was given here.

The enclosed tubular smoldering reactor designed to quantify the limiting oxygen conditions is shown in Fig. 1a. The inner diameter was designed to be 12 cm to minimize the quenching/cooling effect of the wall boundary [15,27]. Meanwhile, the tubular reactor was further enveloped by a 2-cm thick thermal-insulation material and an aluminum foil layer to minimize the lateral heat loss. The overall height of the reactor was 30 cm, including three parts (from top to bottom): (1) insulation zone (5 cm), (2) combustion zone (15 cm), and (3) gas homogenization system (10 cm) (see Fig. 1a). Oxidizer flows with various flow velocities (U, mm/s) and oxygen concentrations (X_{O_2} (volume fraction) or Y_{O_2} (mass fraction), %) were fed from the bottom. An array of eight K-type thermocouple probes (1-mm bead diameter) with an interval of 2 cm was placed vertically at the central axis of the fuel. It is noteworthy that the ignition protocol of the experiments used to validate this model differs from that described in the [38]. Instead, a top-ignition approach was employed (see Fig. 1b and c). The reason was to avoid (1) the complex bidirectional propagation in middle ignition scenarios (Fig. 1d), and (2) weak local burning at the bottom without propagation in bottom ignition scenarios (Fig. 1e). Hence, the oxygen supply or smothering limit of smoldering propagation can be focused. Additionally, to ensure a uniform and robust smoldering front, a supplementary 1-cm thick layer of pine needles, pre-ignited by a propane flame for 1 min, was introduced to the top of the test sample to serve as the ignition source.

Pine needles (see photo in Fig. 1) were used as representative porous media in this work, and they were collected from the larch forest in Saihanwula Biosphere Reserve, China. The natural pine needle bed had

a highly porous structure (porosity = 0.9 ± 0.02), and the thermogravimetric analysis test showed an organic content of > 80 % and a mineral content of about 15 %. All pine needles were pre-dried in ovens at 75 °C for at least 48 h, and the moisture content (MC) was controlled below 5 %, which was demonstrated to have a negligible effect on smoldering propagation [41]. By compressing the fuel bed, bulk densities ranging from 50 ± 10 to 150 ± 30 kg/m^3 were achieved.

For all tests, as the lateral heat loss was minimized to a negligible level, and ignition was applied throughout the entire cross-area surface, the whole vertical smoldering spread can be approximated as a one-dimensional spread process [24]. Therefore, a 1-D computational model with the same sample depth as that in the experiment (refer to Fig. 1a) was established using Gpyro v0.7 [39]. Gpyro is a generalized open-source code for combustible solids and has been used to simulate the pyrolysis and smoldering of various porous media such as peat [27], wood [19], PU foam [39], and coal [42]. Initially, the simulation was started with an excessive oxygen supply. If smoldering can propagate successfully under these conditions, subsequent tests were conducted with reduced oxygen flow rates. Ultimately, the limiting oxygen supply rate will be obtained, below which smoldering cannot be sustained. Following this, oxygen concentrations can be adjusted by changing the ratio of N_2 to O_2, enabling further investigations into the minimum oxygen supply rate under different oxygen concentrations.

2.2. Governing equations

The 1-D computational model solved the transient conservation equations for condensed and gaseous phases in the absence of gravity, since the gravity and buoyancy effect inside the porous media of such a small fuel sample played a negligible role [21,27]. The governing conservation equations were provided here, including the conservation of (1) mass, (2) species, and (3) energy in the condensed phase, as well as the conservation of (4) mass, (5) species, and (6) momentum (Darcy's law) in the gas phase. All symbols were explained in the Nomenclature, and more details can be found in Gpyro technical reference [43]. This model also assumed the thermal equilibrium between gas and condensed-phase species (i.e., local gas and solid species have the same temperature), unit Schmidt number, and the same gas diffusion coefficient and specific heat for all gas species. For simplification, the air was assumed to have a constant density (ρ_g) of 1.161 kg/m^3, regardless of the oxygen mass fraction (Y_{O_2}) or gas temperature (T_g). The effect of sample shrinkage is not included in this model, since it plays a negligible role in the limiting oxygen supply for smoldering combustion. More details of the mathematical form of these equations can be found in [39].

$$\frac{\partial \overline{\rho}}{\partial t} = -\dot{\omega}'''_{fg} \tag{1}$$

$$\frac{\partial(\overline{\rho} Y_i)}{\partial t} = \dot{\omega}'''_{fi} - \dot{\omega}'''_{di} \tag{2}$$

$$\frac{\partial(\overline{\rho}\overline{h})}{\partial t} + \frac{\partial(\dot{m}''\overline{h}_g)}{\partial z} = \frac{\partial}{\partial z}\left(k\frac{\partial T}{\partial z}\right) + \sum \dot{\omega}'''_{di,k}\Delta H_k \tag{3}$$

$$\frac{\partial(\rho_g\overline{\psi})}{\partial t} + \frac{\partial \dot{m}''}{\partial z} = \dot{\omega}'''_{fg} \tag{4}$$

$$\frac{\partial(\rho_g\overline{\psi}Y_j)}{\partial t} + \frac{\partial(\dot{m}'' Y_j)}{\partial z} = -\frac{\partial}{\partial z}\left(\rho_g\overline{\psi}D\frac{\partial Y_j}{\partial z}\right) + \left(\dot{\omega}'''_{fi} - \dot{\omega}'''_{dj}\right) \tag{5}$$

$$\dot{m}'' = -\frac{\overline{K}}{\nu}\frac{\partial \overline{p}}{\partial z}\left(\rho_g = \frac{P\overline{M}}{RT}\right) \tag{6}$$

2.3. Smoldering chemical kinetics and parameter selection

The heterogeneous chemistry of the smoldering pine needles was described by a 5-step kinetic scheme with three major components: hemicellulose, cellulose, and lignin [40]. The 5-steps included (1) drying [*dr*]; (2) pyrolysis of hemicellulose, cellulose, and lignin (the typical temperature at ~250 °C, ~300 °C, and ~350 °C, respectively) [*hp*], [*cp*], [*lp*]; (3) char oxidation [*co*], expressed as:

$$Water \rightarrow Water\ vapor\ [dr] \tag{7}$$

$$Hemicellulose \rightarrow Char + Pyrolyzates\ [hp] \tag{8}$$

$$Cellulose \rightarrow Char + Pyrolyzates\ [cp] \tag{9}$$

$$Lignin \rightarrow Char + Pyrolyzates\ [lp] \tag{10}$$

$$Char\ +\ O_2 \rightarrow Ash + gas\ [co] \tag{11}$$

The normalized destruction rate of condensed-phase species A in reaction k can be expressed by Arrhenius law as

$$\dot{\omega}^*_k = Z_k \exp\left(-\frac{E_k}{RT}\right) f(m^*_A) g(Y_{O_2}) \tag{12}$$

where Z_k is the pre-exponential factor, and E_k is the activation energy. The function for mass action of reactant A is

$$f(m^*_A) = (m^*_A)^{n_k} = \left(\frac{m_A}{m_{sA,0}}\right)^{n_k} \tag{13}$$

where $m_{sA,0}$ is the original mass of the species A, and n_k is the reaction order. The oxidation model considers oxidative pyrolysis as

$$g(Y_{O_2}) = \begin{cases} 1 & (n_{k,O_2} = 0) \\ (1 + Y_{O_2})^{n_{k,O_2}} - 1 & (n_{k,O_2} \neq 0) \end{cases} \tag{14}$$

Physical properties of all condensed-phase species were obtained from [44] and listed in Table 1, where the subscript s and o represents the solid physical properties (i.e., $\psi = 0$) and bulk physical properties, respectively. It is worth noting that compared to fuels with fine particle sizes such as wood dust, pine needle fuel may be more heterogeneously and unevenly distributed in real scenarios. However, this model does not consider such factors and treats pine needles as uniform porous media. Therefore, the effective thermal conductivity in porous media included the radiation heat transfer across pores as

$$k_i = k_{s,i}(1 - \psi_i) + \gamma_i \sigma T^3 \tag{15}$$

Table 1
The physical parameters of condensed-phase species.

Species (i)	Y_0 (−)	$\rho_{s,i}$ (kg/m^3)	$\rho_{o,i}$ (kg/m^3)	$k_{s,i}$ (W/m·K)	$c_{p,i}$ (J/kg·K)
Water	0.05	1000	1000	0.6	4186
Hemicellulose	0.2	782	150	0.2	1500
Cellulose	0.5	694	150	0.2	1500
Lignin	0.25	454	150	0.2	1500
Char	0	500	100	0.05	3000
Ash	0	150	15	0.1	3000

Table 2
Chemical kinetic parameters of 5-setp reaction for pine needles, where the reaction expression is $A_k + \nu_{O_2,k}\, O_2 \rightarrow \nu_{B,k}\, B_k + \nu_{g,k}$ gas, and $\Delta H_k > 0$ means endothermic.

Parameter	dr	hp	cp	lp	co
$lgZ_k(\lg(s^{-1}))$	8.12	8.2	12.4	14.7	11.9
E_k (kJ/mol)	67.8	106	160	236	184
$n_k(-)$	3	1.49	0.95	8.7	1.27
$n_{k,O_2}(-)$	0.252	454	150	0.2	1500
$\nu_{B,k}$(kg/kg)	0	0.24	0.27	0.40	0.06
ΔH_k (MJ/kg)	2.26	0.2	0.5	0.5	−20
$\nu_{O_2,k}$(kg/kg)	0	0.5	0.5	0.5	1.5

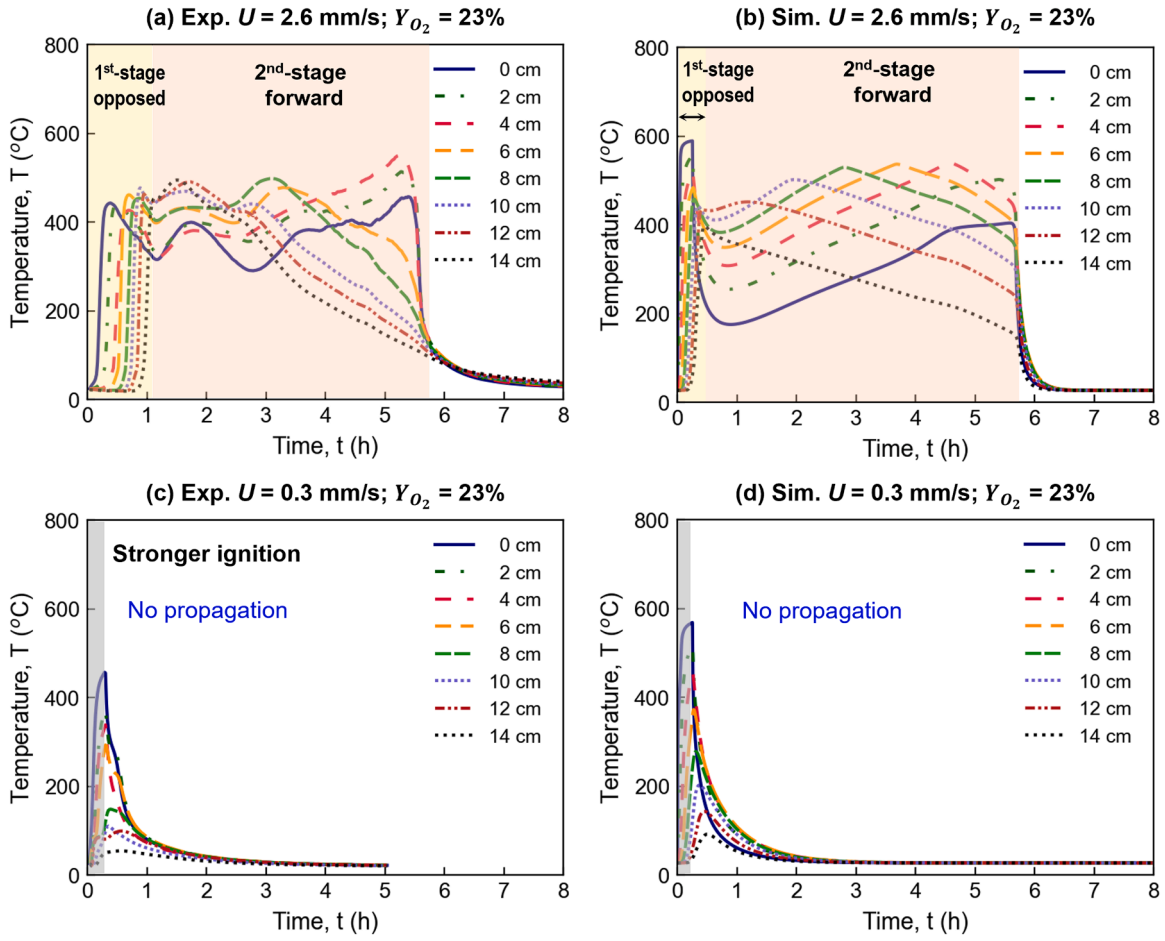

Fig. 2. Comparisons of temperature profiles from experimental measurement and simulations results. (a, b) successful two-stage smoldering propagation under flow velocity of 2.6 mm/s; and (c, d) failed smoldering propagation under insufficient oxygen supply of 0.3 mm/s.

where γ is dependent on the pore size (d_p) as $\gamma \sim d_p = 1/S\rho$. The permeability ($K \sim {d_p}^2$) of all solid species: hemicellulose, cellulose, lignin, char, and ash, was assumed to be independent and estimated on the scale of $10^{-12} \sim 10^{-10}$ [45]. The averaged properties of condensed-phase species in each cell were calculated by weighting appropriate mass or volume fractions as

$$\overline{\rho} = \sum X_i \rho_i,\ \overline{k} = \sum X_i k_i,\ \overline{c} = \sum Y_i c_i,\ X_i = \overline{\rho}\frac{Y_i}{\rho_i} \tag{16}$$

The kinetic and stoichiometric parameters of the 5-step reactions were also obtained from [44] and listed in Table 2.

The initial temperature of the fuel was set to 300 K. To simulate the dried pine needles in the experiments, the MC of fuel was assumed to be 5 %, and the component ratio of was 0.209 (*hemicellulose*): 0.529 (*cellulose*): 0.262 (*lignin*) [44]. The heat transfer coefficient of $h_c = 10$ W/m^{2}K was applied to represent environmental cooling from top and bottom layer, and the emissivity of biomass was set to 0.95. The specific heat capacity (c_g) was assumed to be 1100 J/kg K for all gas species [39]. A forced oxidizer flow was applied from the bottom of the computational domain. To initiate smoldering, a heat flux of 30 kW/m^2 was applied on the top of fuel for the first 5 min. A successful smoldering propagation was defined if the smoldering front can gradually propagate downwards and reach the bottom without any discernible deceleration of propagation or decrease in temperature [15]. To eliminate the influence of inadequate heating on unsuccessful ignition, if no smoldering propagation occurred, the ignition protocol would be progressively enhanced to be 50 kW/m^2 for 30 min. The ambient pressure and temperature were assumed to be 1 atm and 300 K. The solution started to converge at $\Delta Z = 0.1$ mm and $\Delta t = 0.01$ s. Further reducing the cell size and time step by a factor of two gave no significantly different results, so the calculation was sufficiently resolved.

3. Computational results and discussions

3.1. Base cases and model validation

Herein, two base cases (successful and failed self-sustaining smoldering propagation) were first compared between the experiment and the simulation, where the pine needle fuel beds were controlled at $\rho_o = 120 \pm 20$ kg/m^3 and MC = 5 %, and oxygen mass fraction was set at $Y_{O_2} = 23$ %. The example temperature profiles of successful and failed smoldering propagation from experimental and simulation results are compared in Fig. 2. Fig. 2a shows the experimental measurements under an internal airflow velocity of 2.6 mm/s, and the simulated temperature profile is presented in Fig. 2b for comparison. In general, considering the complex nature of the smoldering process, a reasonably good agreement can be observed between computational predictions and experimental data. As depicted in Fig. 2a and b, a two-stage opposed-to-forward smoldering process was observed, consistent with our findings in previous works [7,25]. In the opposed-to-forward propagation, upon ignition from the top, a robust reaction front was established, then a rapid downward propagation was observed, and the reaction front reached the bottom in 1 h. Subsequently, the smoldering front started to spread upward concurrently with the oxidizer flow, which was dominated by the char oxidation process with a longer duration and a higher temperature. After burnout, it was observed from the experimental residues

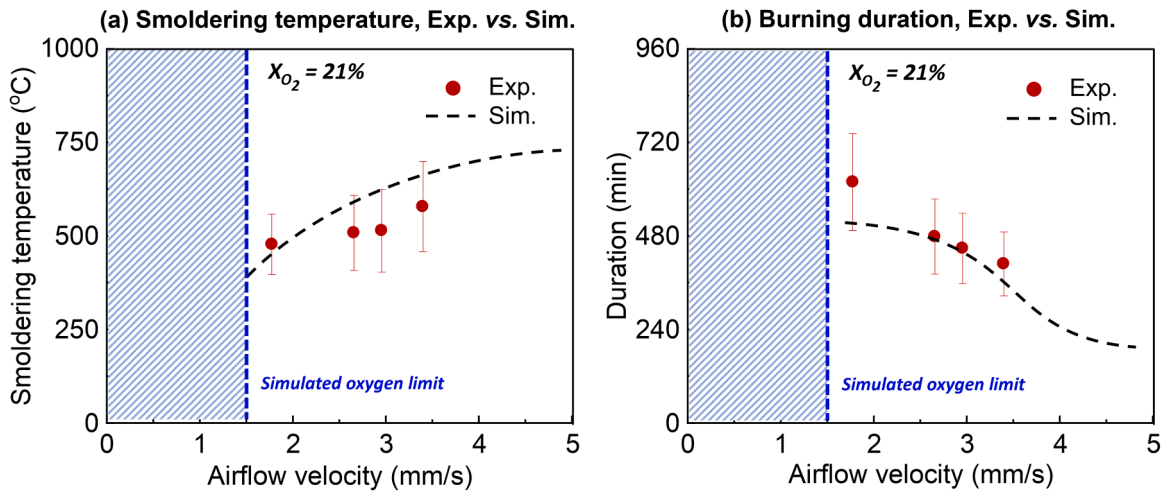

Fig. 3. Comparison of experimental and simulation data on (a) smoldering peak temperature and (b) burning duration. The satisfactory agreement validates the capability of computational model.

that the char and ash formed a fragile structure that didn't collapse naturally. It reduced the surface regression during the burning process, which was different from other smoldering fuels such as peat or tiny wood chips [46]. When the oxygen supply rate was decreased to below the smoldering limit, no propagation occurred in experiments and simulations, as exemplified in Fig. 2c and d. In those scenarios, the insufficient oxygen supply was not able to support the exothermic oxidations that were necessary for the endothermic drying and pyrolysis process. Therefore, after ignition, the system temperatures at all locations drop without any fluctuations.

Note that the "0-cm" probe in Fig. 2a did not read a high temperature instantly like that in Fig. 2b because of the use of an additional "1-cm ignition layer" on the top of the tested fuel bed during experiments (see Section 2.1). Moreover, there was a clear fluctuation in the temperature of the forward spread during experiments (Fig. 2a), possibly due to: (1) non-uniform physicochemical properties of the fuel bed, (2) an uneven smoldering front under oxygen-limited scenarios and (3) random local fuel collapses, which were inevitable in experiments and difficult to be included in the numerical model. Furthermore, the establishment of the model involved many assumptions. For example, the input of physical properties of fuels and their temperature variations were simplified to constants. Also, the model did not consider the microscopic structures of fuel particles and the random local collapses of char and ash during the propagation of smoldering combustion [27]. In addition, the "O_2 leakage" induced by the uneven distribution of fuel was impossible to be included in the model [38]. Therefore, it is impossible to completely match the experimental and simulated results, especially the time-evolution temperature profile [27]. Nevertheless, the shape of the predicted temperature profile, peak temperature, and fire spread duration are consistent with the experimental observations.

Moreover, Fig. 3 further summarizes the simulated peak temperatures and burning durations of smoldering (dash lines), and the experimental results (markers) are plotted for comparison. In general, simulation showed satisfactory agreement with experimental results, and our model is therefore further validated. Notably, the effects of oxidizer flow velocity on the peak temperatures and burning durations were well captured by the model; that is, as the airflow velocity increased, the smoldering temperature increased while the burning duration decreased. It is due to more heat released from oxidation reactions with better oxygen availability, leading to a higher reaction rate. Additionally, the behavior that the same fuel can burn for a longer duration under limited oxygen supply also corresponds to the phenomenon where smoldering fires in deep underground environments can persist for weeks and even months [3,7]. These smoldering

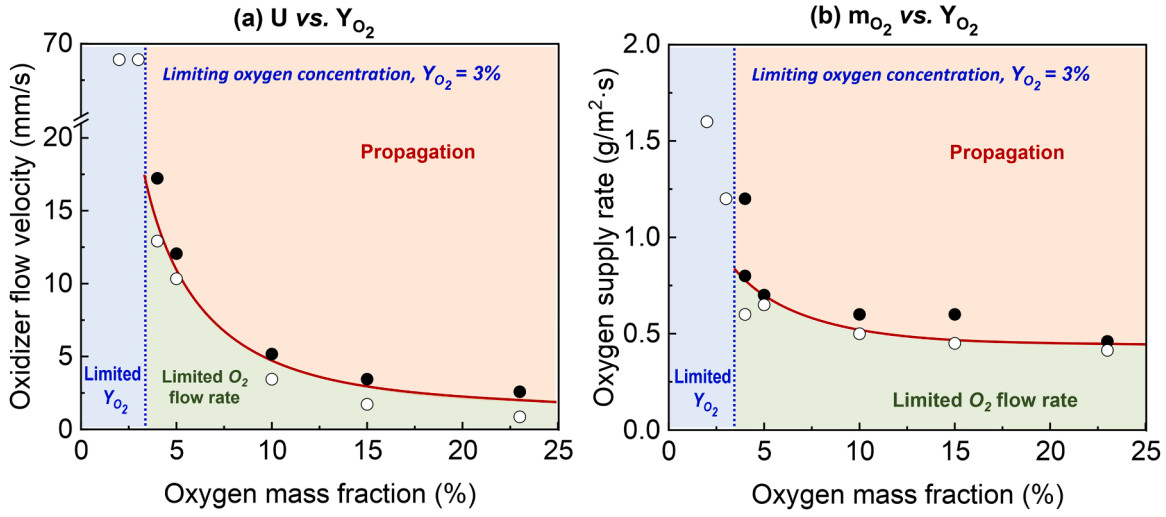

Fig. 4. Simulation results and boundary trendlines of (a) minimum internal flow velocity (U) vs. oxygen mass fraction (Y_{O_2}); (b) minimum oxygen supply rate (m_{O_2}) vs. oxygen mass fraction (Y_{O_2}). The solid (●) and hollow (○) mark represents numerical results of propagation and extinction, respectively.

dynamics in near-limit conditions require further research to be revealed.

Referring to both Figs. 2 and 3, the experiment and simulation results exhibited a strong agreement in terms of propagation mode, spread rate, smoldering temperature, and burning duration. This consistency validates the capability of our model to accurately simulate the propagation and extinction of smoldering combustion driven by oxygen supply in porous pine needle beds.

3.2. Roles of oxygen concentrations

Following the validated model and base cases, we further explored the oxygen thresholds or smothering limits by adjusting the oxygen mass fractions (Y_{O_2}) of internal oxidizer flow. Fig. 4a describes the simulated boundary trendlines for the smothering limits of smoldering combustion, i.e., the minimum internal flow velocity ($U_{\min}$) to sustain smoldering under various Y_{O_2}. First, the LOC was found to be 3 %, below which smoldering was not able to survive, irrespective of the flow velocity. Afterwards, the predicted required flow velocity increased with the decreasing oxygen mass fraction, which was consistent with the trend shown in our previous experimental work on smoldering peat [24]. For example, the predicted required flow velocity increased from 1.6 mm/s to 12 mm/s, as Y_{O_2} decreased from 23 % to 5 %.

Based on previous work [24,26], at the extinction limit, the heat generated from the net heterogeneous smoldering reactions ($\dot{q}''_{sm}$) should just balance the heat loss from water evaporation ($\dot{q}''_{MC}$), internal flow convection $\left(\dot{q}''_{conv,in}\right)$, and environmental heat losses ($\dot{q}''_{e}$) as

$$\dot{q}''_{sm,min} = \dot{q}''_{MC} + \dot{q}''_{conv,in.} + \dot{q}''_{e} \tag{17}$$

By further organizing Eq. (17), we obtain

$$\dot{q}''_{sm,\min} = S_{sm}\rho_w \Delta H_{ev} MC + \rho_g c_{p,g} U(T_{sm} - T_\infty) + (h_r + h_c)(T_{sm} - T_\infty) \tag{18}$$

where S_{sm} and T_{sm} refers to smoldering propagation rate and temperature. For simplicity, the radiative heat loss is linearized by using the radiation heat transfer coefficient (h_r) [47]. On the other hand, the minimum oxidation heat generated can be described as

$$\dot{q}''_{sm,\min} = \dot{q}''_{ox} = \dot{m}''_{O2,\min} \Delta H_{ox} = \rho_g (U Y_{O_2})_{\min} \Delta H_{ox} \tag{19}$$

where ρ_g is the density of oxidizer flow, and ΔH_{ox} is the heat of smoldering oxidation. Therefore, the minimum oxidizer flow velocity and can be derived as

$$U_{\min} = \frac{S_{sm}\rho_w \Delta H_{ev} MC + (h_r + h_c)(T_{sm} - T_\infty)}{\rho_g Y_{O_2} \Delta H_{ox} - \rho_g c_{p,g}(T_{sm} - T_\infty)} \propto \frac{1}{Y_{O_2} - C} \quad (Y_{O_2} > 3\,\%) \tag{20}$$

where for a specific fuel with a particular MC and density, S_{sm} and T_{sm} can be regarded as constants at the limiting condition of smoldering propagation [27]. $C = \frac{c_{p,g}(T_{sm} - T_\infty)}{\Delta H_{ox}}$ is a constant relying on smoldering and ambient temperatures. Therefore, the minimum gas flow velocity is inversely proportional to the oxygen concentration ($U_{\min} \propto \frac{1}{Y_{O_2} - C}$) in Eq. (20), and the overall trend of simulated results in Fig. 4(a) is successfully explained. Furthermore, the predicted oxygen supply rate was further calculated as $\dot{m}''_{o2} = \rho_g Y_{O_2} U$, and the results are shown in Fig. 4b. It is found that $\dot{m}''_{o2}$ increased from 0.45 g/m^2·s to 0.8 g/m^2·s when Y_{O_2} decreased from 23 % to 4 %. This trend also agreed well with the trend found in our previous experiments [24].

3.3. Fuel density, moisture and ambient temperature

Fuel dry bulk density (ρ_{dry}) and moisture content (MC) is expected to vary in applied smoldering systems and wildfire scenarios. More importantly, they were found to play a significant role in the propagation and extinction of smoldering combustion [46]. Herein, the sensitivity of the oxygen thresholds or smothering limits to fuel MC was explored by varying MC within a range of 5 % and 120 % (dry basis). Note that the fuel dry bulk density was controlled as $\rho_{dry} = \rho_{wet}/(1 + \mathrm{MC})$ that the volume expansion from absorbing water can be balanced [46].

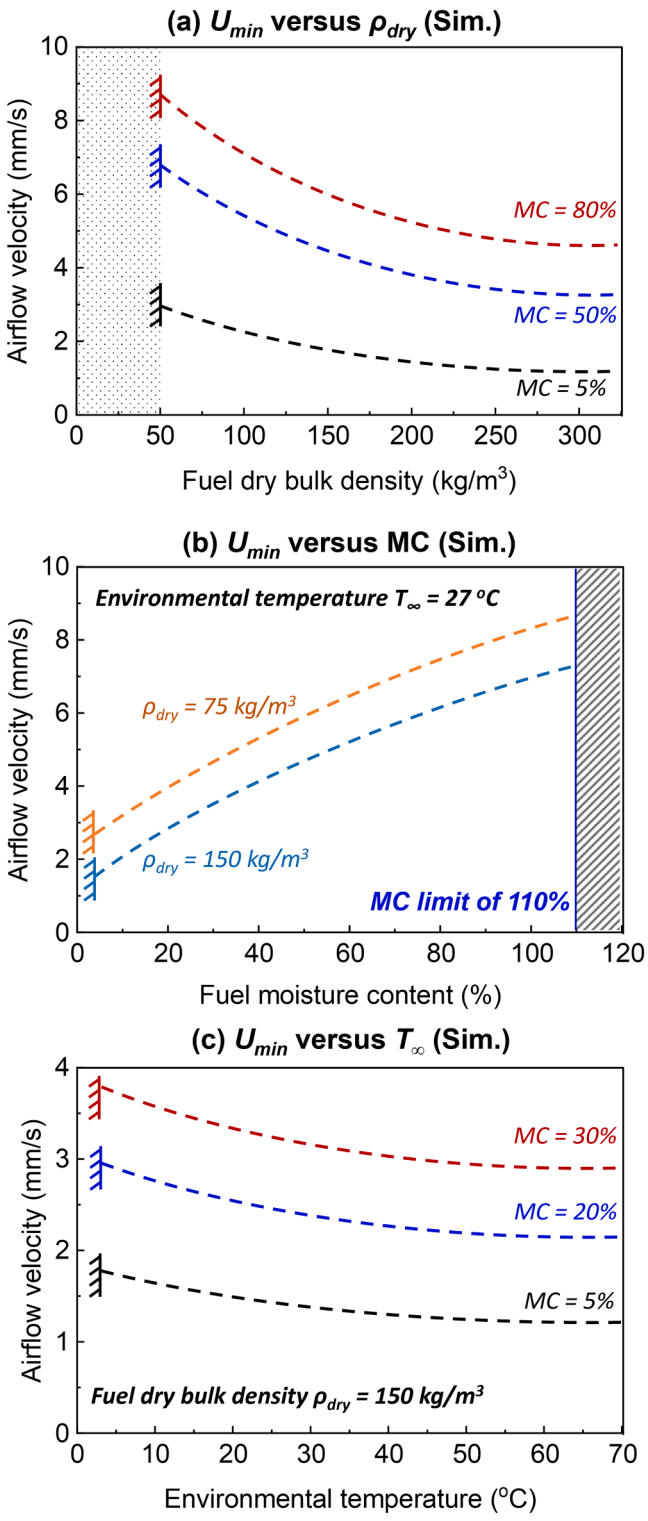

Fig. 5. Simulation results of the role of (a) fuel dry bulk density, (b) moisture content, and (c) ambient temperature on oxygen threshold of smoldering combustion.

Computational results showed that the required airflow velocity was significantly influenced by fuel dry bulk density (Fig. 5a) and MC (Fig. 5b). On the one hand, as the fuel dry bulk density increases, the

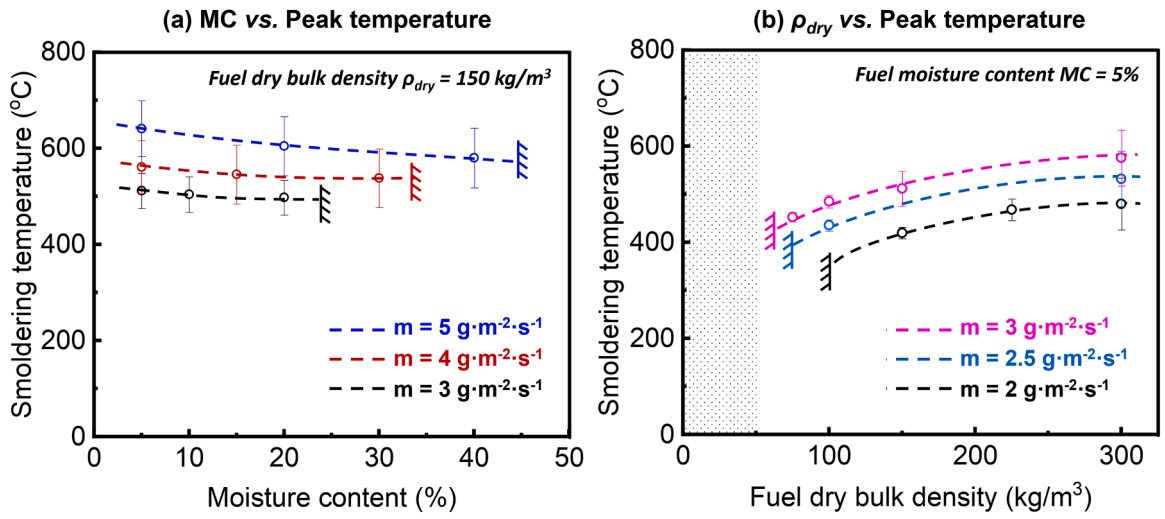

Fig. 6. The (peak) smoldering temperature (T_{sm}) as a function of (a) fuel moisture content and (b) fuel dry bulk density. All curves are trend lines with fixed oxygen supply of simulated results.

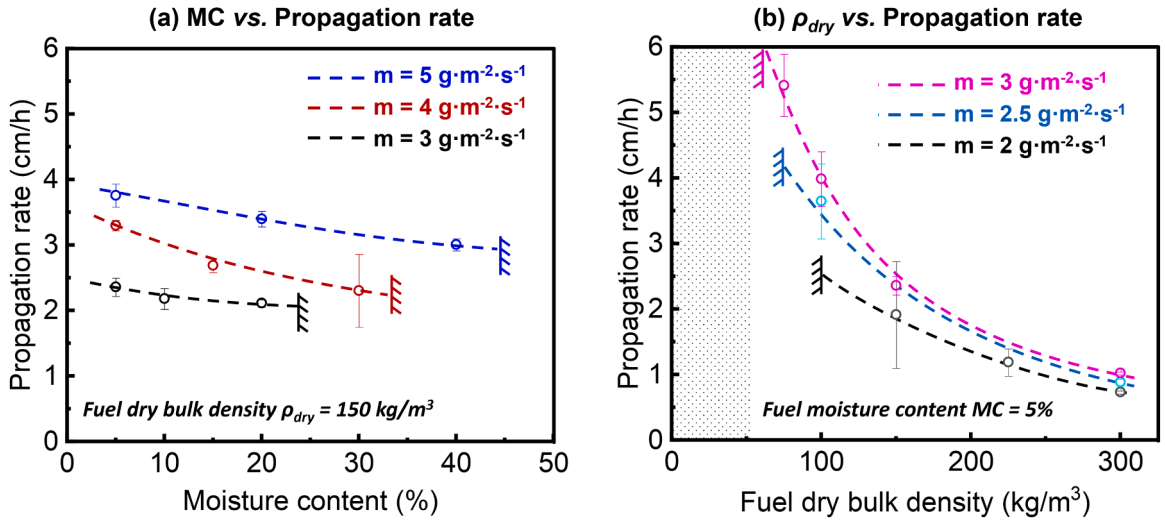

Fig. 7. The smoldering propagation rate (S_{sm}) as a function of (a) fuel moisture content and (b) fuel dry bulk density. All curves are trend lines with fixed oxygen supply of simulated results.

required airflow velocity was predicted to decrease (Fig. 5a), well agreeing with previous findings [38]. For example, when MC is 50 %, as the fuel dry bulk density increases from 50 kg/m^3 to 300 kg/m^3, the airflow velocity required for sustaining smoldering was predicted to decrease from about 7 mm/s to 3 mm/s. As the fuel dry bulk density, the effective thermal conductivity of the fuel will increase [47], thus increasing the heat transfer efficiency between the burning zone and virgin fuels, and lowering the airflow velocity required for sustaining smoldering propagation [38].

On the other hand, as the fuel moisture content increases, the required airflow velocity was predicted to increase, as shown in Fig. 5b. For example, as MC increased from 5 % to 50 %, the required oxygen supply for high-density pine needles ($\rho_{dry} = 150$ kg/m^3) rose from about 2 mm/s to about 5 mm/s. This trend can be also explained by Eq. (20), where $U_{\min}$ increases as $\dot{q}''_{MC}$ increases; that is, a higher airflow velocity is required to intensity the reactions that release more heats to overcome the heat loss due to the water evaporation. Furthermore, the maximum MC capable of supporting smoldering is about 110 % (Fig. 5b). Beyond this limit, smoldering was not able to be sustained regardless of oxygen supply.

In real fire scenarios, the ambient temperature can be much higher which may lead to a different oxygen threshold. Therefore, the effect of ambient temperature (T_∞) was also investigated and summarized in Fig. 5c. In order to focus on the T_∞, the process of water freezing caused by sub-zero temperature was out of the scope of this study. As a result, the temperature range under investigation was limited to 0–70 °C. Predicted results showed that the required airflow velocity decreases as T_∞ increases. For example, given a fixed fuel moisture content of 5 %, as the ambient temperature increases from 10 °C to 70 °C, the predicted required airflow velocity decreases from about 1.7 mm/s to about 1.4 mm/s. This could be also explained by Eqs. (17) and (18), where the convective and radiative heat loss will decrease as T_∞ increases, leading to a lower airflow velocity required for self-sustaining smoldering propagation.

3.4. Smoldering temperature (T_{sm}) and propagation rate (S_{sm})

Smoldering temperature (T_{sm}) and propagation rate (S_{sm}) are two key parameters that describe the smoldering behaviors and reflect the intensities of reactions and the rates of fuel consumption. Therefore, Figs. 6 and 7 further compare the effects of moisture content and bulk

density on the T_{sm} and S_{sm}, and each curve was controlled to have the same airflow mass supply rate (i.e., $\dot{m}''_{O_2}$). First of all, at the smothering limit, the minimum smoldering temperature and propagation rate were predicted to be around 300 °C and 0.5 cm/h, and the predicted T_{sm} and S_{sm} both increase as $\dot{m}''_{O_2}$ increases, agreeing well with the literature [48–50]. By considering a 1-step global smoldering reaction, the smoldering burning flux can be described as

$$\dot{m}''_F = \rho S_{sm} = \frac{\dot{m}''_{O_2}}{\nu} \propto T_{sm} \tag{21}$$

where ν is the stoichiometric factor. By further reorganizing Eq. (21), we obtain

$$S_{sm} = \frac{\dot{m}''_F}{\rho} = \frac{\dot{m}''_{O_2}}{\nu\rho} \tag{22}$$

Therefore, as the $\dot{m}''_{O_2}$ increases, the reaction rate of smoldering combustion increases, leading to a higher smoldering temperature and spread rate.

Furthermore, Fig. 6 shows the smoldering peak temperature will decrease with (a) the increase of moisture content or (b) the decrease of dry bulk density in pine needle beds, while Fig. 7 shows the predicted smoldering propagation rate will decrease as the moisture content and bulk density increase. On the one hand, as the moisture content increases, extra heat is required to dry the fuel before ignition and propagation, leading to a lower smoldering temperature and propagation rate. On the other hand, from Eq. (15), if the density of fuel (ρ) increases, both γ and k_i will decrease. This leads to a higher smoldering temperature but a lower propagation rate as the heat is easier to accumulate and more difficult to dissipate within the fuel due to a lower thermal conductivity [38], consistent with the trend shown in Figs. 6 and 7. Moreover, it is noteworthy that the smoldering temperature is more sensitive to the oxygen supply rather than moisture content and bulk density, agreeing with previous studies [46]. For example, when the air flow rate was stabilized at 3 g/m^2 s, as the moisture content was reduced from 20 % to 5 %, the smoldering temperature was only decreased by 20 °C. However, if the air flow rate was increased from 3 g/m^2-s to 5 g/m^2 s, the smoldering peak temperature was significantly increased by 100 °C. Nevertheless, more fundamental studies are still needed to unravel the underlying mechanisms governing the smoldering propagation.

4. Conclusions

In this work, we employed numerical simulations to investigate the oxygen supply thresholds or smothering limits of smoldering combustion of pine needle beds. The model integrating heat-and-mass transfer and 5-step heterogeneous chemistry was established using open-source code Gpyro and was successfully validated through well-controlled experiments. Subsequently, the required oxidizer flow velocity or oxygen supply rate was predicted to increase as the oxygen concentration decreased. Notably, the predicted limiting oxygen concentration specially for smoldering combustion was about 3 %, agreeing well with both the experimental observations and theoretical analysis.

Then, the sensitivity of the oxygen thresholds or smothering limits to fuel density, moisture content and environmental temperature was further explored. Computational results revealed that the required airflow velocity for smoldering combustion increased as the fuel density or environmental temperature decreased. However, the required airflow velocity was predicted to increase as the moisture content increased, and the predicted maximum moisture content capable of supporting smoldering was about 110 %.

Finally, the smoldering peak temperature was predicted to decrease as the moisture content increased or the bulk density decreased, while the predicted smoldering propagation rate was predicted to decrease as the moisture content and bulk density increase, consistent with the theoretical analysis. At the smothering limit, the minimum smoldering temperature and propagation rate were predicted to be around 300 °C and 0.5 cm/h. This work improves our understanding of thresholds of propagation and smothering of smoldering combustion, thus helping mitigate smoldering fire risk and optimize the applied smoldering processes.

CRediT authorship contribution statement

Yunzhu Qin: Writing – original draft, Resources, Methodology, Investigation, Formal analysis, Data curation. **Yuying Chen:** Resources, Formal analysis. **Yichao Zhang:** Resources, Formal analysis. **Shaorun Lin:** Writing – review & editing, Resources, Methodology, Formal analysis, Data curation. **Xinyan Huang:** Writing – review & editing, Supervision, Resources, Project administration, Funding acquisition.

Declaration of competing interest

The authors declare that they have no known competing financial interests or personal relationships that could have appeared to influence the work reported in this paper.

Acknowledgments

This research is funded by the National Natural Science Foundation of China (No. 52322610), and RGC Hong Kong GRF Scheme (No. 15221523).

References

[1] G. Rein, Smoldering combustion. SFPE Handb. Fire Prot. Eng. Fifth Ed, Elsevier, New York, NY, 2016, pp. 581–603.
[2] T.J. Ohlemiller, Modeling of smoldering combustion propagation, Prog. Energy Combust. Sci. 11 (1985) 277–310.
[3] G. Rein, Smouldering Fires and Natural Fuels, in: C.M. Belcher (Ed.), Fire Phenom. Earth Syst. An Interdiscip. Guid. to Fire Sci., WileyBlackwell, London, 2013, pp. 15–33.
[4] J.L. Torero, J.I. Gerhard, M.F. Martins, M.A.B. Zanoni, T.L. Rashwan, J.K. Brown, Processes defining smouldering combustion: integrated review and synthesis, Prog. Energy Combust. Sci. 81 (2020) 100869.
[5] A. Anca-Couce, N. Zobel, A. Berger, F. Behrendt, Smouldering of pine wood: kinetics and reaction heats, Combust. Flame 159 (2012) 1708–1719.
[6] Z. Song, Modelling oxygen-limited and self-sustained smoldering propagation: underground coal fires driven by thermal buoyancy, Combust. Flame 245 (2022) 112382.
[7] Y. Qin, D.N.S. Musa, S. Lin, X. Huang, Deep peat fire persistently smouldering for weeks : a laboratory demonstration, Int. J. Wildl. Fire 32 (2022) 86–98.
[8] Z. Song, C. Kuenzer, Coal fires in China over the last decade: a comprehensive review, Int. J. Coal Geol. 133 (2014) 72–99.
[9] J. Yang, H. Wang, R. Wang, Z. Fu, Y. Hu, Experimental study of smouldering combustion and transient emissions from forest duff with dual layers, Proc. Combust. Inst. 40 (2024) 105354.
[10] J. Yang, G. Rein, H. Chen, M. Zammarano, Smoldering propensity in upholstered furniture: effects of mock-up configuration and foam thickness, Appl. Therm. Eng. 181 (2020) 115873.
[11] H. Mitchell, R. Amin, M. Heidari, P. Kotsovinos, G. Rein, Structural hazards of smouldering fires in timber buildings, Fire Saf. J. 140 (2023) 103861.
[12] M. Toledo, A. Arriagada, N. Ripoll, E.A. Salgansky, M.A. Mujeebu, Hydrogen and syngas production by hybrid filtration combustion: progress and challenges, Renew. Sustain. Energy Rev. 177 (2023) 113213.
[13] T.L. Rashwan, J.L. Torero, J.I. Gerhard, Heat losses in a smouldering system: the key role of non-uniform air flux, Combust. Flame 227 (2021) 309–321.
[14] J. Li, Q. Zhao, M. Si, Z. Dong, J. Huang, Y. Li, X. Hu, S. Tian, Removal of cadmium in contaminated soils by self-sustaining smoldering, J. Environ. Chem. Eng. 11 (2023) 109869.
[15] S. Lin, X. Huang, Quenching of smoldering: effect of wall cooling on extinction, Proc. Combust. Inst. 38 (2021) 5015–5022.
[16] T.L. Rashwan, J.L. Torero, J.I. Gerhard, Heat losses in applied smouldering systems: sensitivity analysis via analytical modelling, Int. J. Heat Mass Transf. 172 (2021) 121150.
[17] M.A. Decker, D.A. Schult, Dynamics of smoulder waves near extinction, Combust. Theory Model. 8 (2004) 491–512.
[18] J. Yang, N. Liu, H. Chen, W. Gao, R. Tu, Effects of atmospheric oxygen on horizontal peat smoldering fires: experimental and numerical study, Proc. Combust. Inst. 37 (2019) 4063–4071.
[19] F. Richter, F.X. Jervis, X. Huang, G. Rein, Effect of oxygen on the burning rate of wood, Combust. Flame 234 (2021) 111591.

[20] R.M. Hadden, G. Rein, C.M. Belcher, Study of the competing chemical reactions in the initiation and spread of smouldering combustion in peat, Proc. Combust. Inst. 34 (2013) 2547–2553.
[21] X. Huang, G. Rein, Interactions of Earth's atmospheric oxygen and fuel moisture in smouldering wildfires, Sci. Total Environ. 572 (2016) 1440–1446.
[22] C.M. Belcher, J.M. Yearsley, R.M. Hadden, J.C. McElwain, G. Rein, Baseline intrinsic flammability of Earth's ecosystems estimated from paleoatmospheric oxygen over the past 350 million years, Proc. Natl. Acad. Sci. USA 107 (2010) 22448–22453.
[23] O. Kadowaki, M. Suzuki, K. Kuwana, Y. Nakamura, G. Kushida, Limit conditions of smoldering spread in counterflow configuration: extinction and smoldering-to-flaming transition, Proc. Combust. Inst. 38 (2021) 5005–5013.
[24] Y. Qin, Y. Chen, S. Lin, X. Huang, Limiting oxygen concentration and supply rate of smoldering propagation, Combust. Flame 245 (2022) 112380.
[25] X. Huang, G. Rein, Upward-and-downward spread of smoldering peat fire, Proc. Combust. Inst. 37 (2019) 4025–4033.
[26] A. Bar-Ilan, G. Rein, D.C. Walther, A.C. Fernandez-Pello, J.L. Torero, D.L. Urban, The effect of buoyancy on opposed smoldering, Combust. Sci. Technol. 176 (2004) 2027–2055.
[27] S. Lin, H. Yuan, X. Huang, A computational study on the quenching and near-limit propagation of smoldering combustion, Combust. Flame 238 (2022) 111937.
[28] J.L. Dupuy, Slope and fuel load effects on fire behaviour :laboratory experiments in pine needles fuel beds, Int. J. Wildl. Fire 5 (1995) 153–164.
[29] P.A. Santoni, P. Bartoli, A. Simeoni, J.L. Torero, Bulk and particle properties of pine needle fuel beds-influence on combustion, Int. J. Wildl. Fire 23 (2014) 1076–1086.
[30] Y. Qiao, H. Zhang, J. Yang, H. Chen, N. Liu, M. Xu, L. Zhang, Transition from smouldering to flaming combustion of pine needle fuel beds under natural convection, Proc. Combust. Inst. 40 (2024) 105343.
[31] J.C. Thomas, A. Simeoni, M. Gallagher, N. Skowronski, An experimental study evaluating the burning dynamics of pitch pine needle beds using the FPA, Fire Saf. Sci. 11 (2014) 1406–1419.
[32] S. Benkorichi, T. Fateh, F. Richard, J.L. Consalvi, A. Nadjai, Investigation of thermal degradation of pine needles using multi-step reaction mechanisms, Fire Saf. J. 91 (2017) 811–819.
[33] H. Wang, P.J. van Eyk, P.R. Medwell, C.H. Birzer, Z.F. Tian, M. Possell, Effects of oxygen concentration on radiation-aided and self-sustained smoldering combustion of Radiata pine, Energy Fuels 31 (2017) 8619–8630.
[34] J.P. Valdivieso, J. de Dios Rivera, Effect of wind on smoldering combustion limits of moist pine needle beds, Fire Technol 50 (2014) 1589–1605.
[35] D. Morvan, M. Larini, Modeling of one dimensional fire spread in pine needles with opposing air flow, Combust. Sci. Technol. 164 (2001) 37–64.
[36] J. Yang, H. Wang, R. Wang, J. Xu, W. Huang, Y. Hu, Experimental and theoretical study on the smoldering combustion of size-fractioned forest duff particles, Int. J. Heat Mass Transf. 231 (2024) 125883.
[37] W. Gong, J. Cuevas, P. Reszka, A. Simeoni, The role of smoldering in the ignition of *Pinus palustris* needles, Fire Saf. J. 143 (2024) 104053.
[38] Y. Qin, Y. Zhang, Y. Chen, S. Lin, X. Huang, Minimum oxygen supply rate for smouldering propagation : effect of fuel bulk density and particle size, Combust. Flame 261 (2024) 113292.
[39] C. Lautenberger, C. Fernandez-Pello, Generalized pyrolysis model for combustible solids, Fire Saf. J. 44 (2009) 819–839.
[40] A.K. Rana, S. Guleria, V.K. Gupta, V.K. Thakur, Cellulosic pine needles-based biorefinery for a circular bioeconomy, Bioresour. Technol. 367 (2023) 128255.
[41] X. Huang, G. Rein, Computational study of critical moisture and depth of burn in peat fires, Int. J. Wildl. Fire 24 (2015) 798–808.
[42] H. Yuan, F. Restuccia, F. Richter, G. Rein, A computational model to simulate self-heating ignition across scales, configurations, and coal origins, Fuel 236 (2019) 1100–1109.
[43] C. Lautenberger, Gpyro—A generalized pyrolysis model for combustible solids: technical reference, Berkeley, 2014.
[44] S. Lin, S. Wang, X. Huang, Modeling smoldering ignition by an irradiation spot, Fire Saf. J. 134 (2022) 103708.
[45] X. Huang, G. Rein, Thermochemical conversion of biomass in smouldering combustion across scales: the roles of heterogeneous kinetics, oxygen and transport phenomena, Bioresour. Technol. 207 (2016) 409–421.
[46] X. Huang, G. Rein, Downward spread of smouldering peat fire: the role of moisture, density and oxygen supply, Int. J. Wildl. Fire 26 (2017) 907–918.
[47] F.P. Incropera, Principles of Heat and Mass Transfer, Hoboken, NJ : Wiley. U.S., 2007.
[48] W. Zhang, Q. Song, X. Wang, X. Wang, H. Li, Z. Yang, Experimental study and modeling analysis of sewage sludge smoldering combustion at different airflow rates, Waste Manag. 168 (2023) 126–136.
[49] L. Yermán, H. Wall, J. Torero, J.I. Gerhard, Y.L. Cheng, Smoldering Combustion as a Treatment Technology for Feces: sensitivity to Key Parameters, Combust. Sci. Technol. 188 (2016) 968–981.
[50] Z. Song, B. Dang, H. Zhang, C. Zhao, Y. Xiao, S. Ren, Gas-solid oxygen and thermal nonequilibria of reverse smoldering combustion wave, Proc. Combust. Inst. 40 (2024) 105422.